Bulletin of the Seismological Society of America, Vol. 101, No. 6, pp. 2634–2642, December 2011, doi: 10.1785/0120110016

Resolution of Seismic-Moment Tensor Inversions from a Single Array of Receivers

by Ismael Vera Rodriguez, Yu J. Gu, and Mauricio D. Sacchi

Abstract Moment tensor inversion techniques are widely used in global and regional seismic applications. When the ray-path trajectories are confined in a single plane (e.g., in isotropic media using a vertical array of receivers or an array that deviates from the vertical in the direction of wave propagation) only five out of six elements of the moment tensor are resolvable. This study investigates the resolvability of the complete seismic moment tensor for single-well monitoring geometries. By analyzing the resolution matrix, we demonstrate that a correct representation of the five resolvable elements of the moment tensor is only possible in a local reference system. For a vertical array of receivers, a suitable choice of condition number can assist the acquisition design. For a non-vertical array, our numerical modeling experiments suggest that the required distance and orientation of receivers for a full moment tensor inversion can be satisfied in a deviated well. In this case, information embedded in the condition number is valuable for determining the required distribution of receivers along the well.

Introduction

Determination of the seismic moment tensor is a routine procedure in earthquake seismology (e.g., Dziewonski *et al.*, 1981; Dreger and Helmberger, 1993; Kawakatsu, 1995; Zhao and Helmberger, 1994). Since the mid 1990s, the worldwide increase in seismic networks has facilitated real-time or near real-time extraction of the six tensor elements (Dreger and Helmberger, 1993; Pasyanos *et al.*, 1996). Today, fast solutions for both regional and teleseismic earthquakes are reported by various institutions (e.g., Dziewonski *et al.*, 1981; Sipkin, 1994; Bernardi *et al.*, 2004; Tsuruoka *et al.*, 2009). Moment tensor inversions are less frequently performed for the purposes of monitoring microseismic events induced by hydraulic fractures in oil and gas wells (Nolen-Hoeksema and Ruff, 2001; Rutledge and Phillips, 2003; Bleakly *et al.*, 2007; Jechumtalova and Eisner, 2008). Restrictions in acquisition geometry represent a considerable challenge for daily applications of moment tensor inversions in microseismic monitoring. While microseismic monitoring from multiple wells and/or surface receivers has been adopted (Bleakly *et al.*, 2007; Kolinsky *et al.*, 2009), the single-well approach remains the most common practice. Like most inverse problems, an essential metric in moment tensor determination is resolvability. For a given acquisition geometry and seismic noise level, proper resolvability analyses assess if unknown parameters can be accurately retrieved from an inversion (Menke, 1989). Assessments of resolvability are routinely provided in, for example, studies of free oscillations (Wiggins, 1972), body and surface wave tomography (Trampert, 1998; Rao *et al.*, 2006; Xia *et al.*, 2008), and amplitude-versus-offset (Jing and Rape, 2004). Dufumier and Rivera (1997) estimated the resolvability of the isotropic component of the seismic moment tensor for surface stations. Trifu and Shumila (2002) investigated the accuracy of inverted source mechanisms, which is crucial for assessing risks associated with mining activities, based on statistical reliability. Resolvability of the full moment tensor for data acquired during microseismic monitoring surveys has been discussed in both single (Nolen-Hoeksema and Ruff, 2001; Vavrycuk, 2007) and multiple (Vavrycuk, 2007) vertical wells. For the case of a single vertical well, the array of receivers is assumed to reside within a plane containing the hypocenter of a given source (which we refer to as the observational plane). In isotropic and certain anisotropic (e.g., vertical transverse isotropic) media, only five of the six elements of the moment tensor can be independently determined (Vavrycuk, 2007). The same restriction applies for a well that deviates from the vertical (deviated well) in the direction of wave propagation. In short, Nolen-Hoeksema and Ruff (2001) and Vavrycuk (2007) provide a blueprint for the inversion of the moment tensor in microseismic monitoring applications.

This study examines the resolvability of full moment tensor inversions under single-well monitoring geometries. In vertical geometries, our experiments demonstrate that solutions of the moment tensor are only correctly represented in a reference system with two of its axes constrained to the observational plane (for short, the aligned system). Rotation

of the tensor elements to a different reference system requires correct values for the dipole perpendicular to the observational plane; errors will propagate to two other moment tensor elements otherwise. Through a careful analysis on nonplanar source–receivers geometries and condition numbers, we aim to provide quantitative criteria for resolving five and six moment tensor elements in vertical and deviated wells, respectively.

Parameterization

For an elastic homogeneous medium, the far-field displacement at a distant station can be expressed as a function of the seismic moment tensor (Shearer, 1999, equations 9.13 and 9.17),

$$u_{i(P|S)}(\mathbf{x},t)=\left(\frac{1}{4\pi\rho c^3}\right)\left(\frac{1}{r}\right)R_{ijk(P|S)}\dot{M}_{jk}\left(t-\frac{r}{c}\right), \quad (1)$$

where u_i is displacement recorded on the ith component of a receiver at a specific time t and position $\mathbf{x}$, and $(P|S)$ refers to compressional or shear waves. In this formulation ρ is the density of the medium, c is the speed of P or S waves, and r is the distance between the source and receiver. We use R_{ijk} to represent the radiation pattern defined by the jkth element of the moment rate tensor $\dot{M}_{jk}$ along the ith component of a receiver. We also adopt the reference system of Aki and Richards (2009), where the x_1, x_2, and x_3 components point north, east, and downward, respectively. Integrating both sides of equation (1) over the source duration (τ), we have

$$\int_\tau u_{i(P|S)}dt=\left(\frac{1}{4\pi\rho c^3}\right)\left(\frac{1}{r}\right)R_{ijk(P|S)}\int_\tau \dot{M}_{jk}\left(t-\frac{r}{c}\right)dt, \quad (2)$$

where

$$\int_\tau \dot{M}_{jk}\left(t-\frac{r}{c}\right)dt=M_{jk}. \quad (3)$$

In equation (3), M_{jk} is the jkth element of the seismic moment tensor of the source. Equation (2) can be written in matrix notation as

$$\mathbf{d}_{(P|S)}=\mathrm{K}_{(P|S)}\mathbf{X}_{(P|S)}\mathbf{m}=\mathbf{A}_{(P|S)}\mathbf{m}, \quad (4)$$

where $\mathbf{d}_{(P|S)}$ are the integrals of the displacement at each receiver component arranged in column vector form, $\mathrm{K}_{(P|S)}$ are constants that depend on the medium properties, and $\mathbf{X}_{(P|S)}$ are matrices containing the radiation pattern. In this expression the six independent elements of the moment tensor have been arranged in the column vector $\mathbf{m}=(M_{11},M_{12},M_{13},M_{22},M_{23},M_{33})$. For P and S waves recorded by multiple receivers, one can rewrite equation (4) to a more compact form,

$$\mathbf{d}=\mathbf{A}\mathbf{m}. \quad (5)$$

Our objective is to retrieve the seismic moment tensor $\mathbf{m}$ from observations $\mathbf{d}$. The least squares solution to equation (5) requires the inverse of the matrix $\mathbf{G}=\mathbf{A}^T\mathbf{A}$. The following sections provide detailed analyses on the stability conditions of the inverse problem.

Resolution under Single Vertical-Monitoring Well Geometries

Resolution Matrix

We analyze the resolvability of the inverse problem presented in the previous section by using a model resolution matrix (Van Rijssen and Herman, 1991; Dufumier and Rivera, 1997; Jing and Rape, 2004; Vera Rodriguez and Sacchi, 2009) for single vertical-monitoring well geometries (Figure 1). The symmetric matrix $\mathbf{G}$ admits the eigendecomposition

$$\mathbf{G}=\mathbf{X}\mathbf{\Lambda}\mathbf{X}^T,$$

where $\mathbf{\Lambda}$ is a diagonal matrix of the eigenvalues of $\mathbf{G}$ and $\mathbf{X}$ contains the corresponding eigenvectors. The positive semidefinite nature of $\mathbf{G}$ ensures that its eigenvalues are real and nonnegative (Anton and Busby, 2003). The pseudoinverse of $\mathbf{G}$ can be written as

$$\mathbf{G}^\dagger=\mathbf{X}\mathbf{\Lambda}^\dagger\mathbf{X}^T,$$

where $\mathbf{\Lambda}^\dagger$ is the pseudoinverse of $\mathbf{\Lambda}$ with the positive eigenvalues of $\mathbf{G}$ replaced by their reciprocals (Horn and Johnson, 1985). The resolution of the system in equation (5) is estimated from the pseudoinverse of matrix $\mathbf{G}$,

$$\hat{\mathbf{m}}=(\mathbf{G})^\dagger\mathbf{A}^T\mathbf{d}.$$

For noise-free data, we substitute equation (5) in the last expression and obtain

$$\hat{\mathbf{m}}=\mathbf{G}^\dagger\mathbf{G}\mathbf{m}.$$

The product $\mathbf{G}^\dagger\mathbf{G}$ is the model resolution matrix (Aster *et al.*, 2005); that is

$$\mathbf{R}=\mathbf{G}^\dagger\mathbf{G}.$$

Matrix $\mathbf{R}$ becomes the identity matrix when $\mathbf{G}^\dagger=\mathbf{G}^{-1}$, when all the model components are linearly independent and accurately determined (i.e., $\hat{\mathbf{m}}=\mathbf{m}$). If $\mathbf{G}^\dagger\neq\mathbf{G}^{-1}$, then $\mathbf{R}$ provides important information on the resolvability of the model elements. For example, the existence of nonzero off-diagonal components ($\mathbf{R}_{ij}\neq 0$) implies a linear correlation between model parameters m_i and m_j.

Numerical Test. We begin our numerical simulations by adopting a homogeneous medium with velocities $\alpha=2500\ \frac{\mathrm{m}}{\mathrm{s}}$, $\beta=1400\ \frac{\mathrm{m}}{\mathrm{s}}$, and density $\rho=2.5\ \frac{\mathrm{g}}{\mathrm{cm}^3}$. Eight receivers are placed in a vertical array with separations of 30 m. We vary the horizontal distance between the array

of receivers and the source hypocenter (d) in steps of 10 m between 100 and 700 m, and examine array azimuths (see Fig. 1) from $-\pi$ to π in steps of $\frac{\pi}{24}$ radians. The geographical reference system is used in this part of the analysis, though the main outcomes are equally applicable to other fixed reference systems. The resolvability of the model parameters is insensitive to the distance between the line of receivers and the source hypocenter (Fig. 2). However, different model parameters become linearly correlated when the azimuth of the line of receivers is altered. Five out of six model parameters can be correctly estimated when the observational plane is aligned with two axes of the geographical reference system, though the dipole perpendicular to the observational plane is not fully resolvable (see also Nolen-Hoeksema and Ruff, 2001; Vavrycuk, 2007). Representation of model parameters M_{13}, M_{23}, and M_{33} are proper for all θ and d, but the resolution matrix suggests undesired correlations between M_{11}, M_{12}, and M_{22} when the observational plane is misaligned with the geographical reference system. These results, which are obtained in a homogeneous medium, are equally valid for layered and anisotropic media, provided that the travel paths of the seismic energy recorded at the receivers are contained in the observational plane (Vavrycuk, 2007).

Maximum Number of Resolvable Elements

It has been discussed that, without additional assumptions in the expected solutions, only five out of six independent elements of the seismic moment tensor are retrievable in single vertical-monitoring well geometries. The existence of a null eigenvalue in the sensitivity matrix (**G**) causes instability

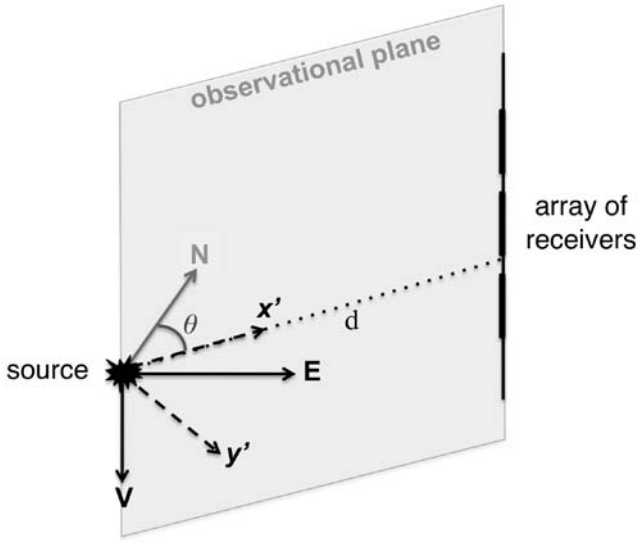

Figure 1. Source–receivers geometry for the microseismic monitoring experiment with one vertical-monitoring well. The geographical and aligned reference systems have axes north (N), east (E), and vertical (V), and x', y', and V, respectively. The axes x' and V are contained in the observational plane. The angle θ denotes the azimuth of the array of receivers (receiver azimuth) from North.

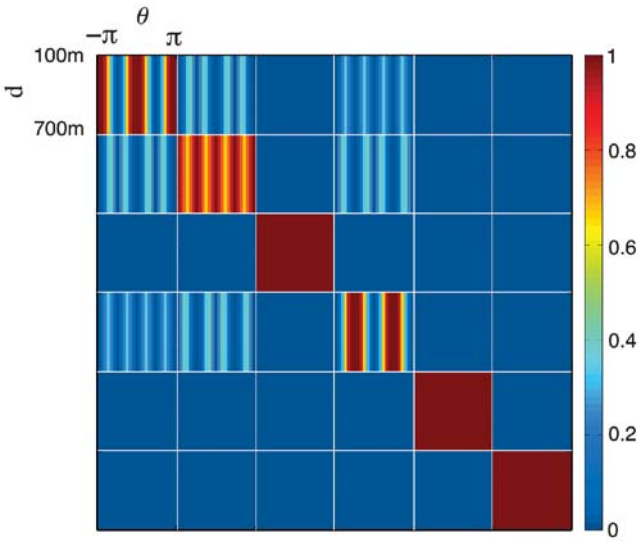

Figure 2. Resolution matrix for different combinations of source–receivers horizontal distance (d) and azimuth of the line of receivers (θ). Each diagonal box (delimited by white lines) represents the resolvability of the seismic moment tensor elements in the order M_{11}, M_{12}, M_{13}, M_{22}, M_{23}, and M_{33} (equivalently, m_1, m_2, m_3, m_4, m_5, and m_6). The scales shown on box R_{11} apply for any other box of the matrix. Colors close to one in a diagonal box mean that the corresponding element can be solved in the inversion. Colors different from zero in off-diagonal boxes (R_{ij}) denote the linear dependency between the corresponding elements of the seismic moment tensor (m_i and m_j).

in the inversion process. The most common approach to minimize this instability is to seek deviatoric solutions (Dufumier and Rivera, 1997). This strategy does not guarantee the correctness of the solutions, however (Vavrycuk, 2007). It was first proposed that induced events during hydraulic fracturing were mainly deviatoric or double couples (Phillips *et al.*, 1998; Rutledge and Phillips, 2003), though more recent studies have further suggested the presence of tensile events (Jechumtalova and Eisner, 2008; Sileny *et al.*, 2009). Constrained inversions do not assist us in identifying tensile events. Furthermore, tensile events can be mistakenly fitted by deviatoric sources. The plausibility of a constrained inversion in microseismic monitoring is an important subject that requires an in-depth analysis beyond the scope of this study.

The resolution matrix shows that seismic moment tensor solutions in single vertical-monitoring well geometries are only correctly represented in the aligned reference system (unless the value of the dipole perpendicular to the observational plane is known). In this study we write

$$\mathbf{d} = \mathbf{A}\mathbf{R}_{m\theta}^{-1}\mathbf{m}_\theta, \tag{6}$$

where

$$\mathbf{m}_\theta = \mathbf{R}_{m\theta}\mathbf{m}$$

and

$$\mathbf{R}_{m\theta} = \begin{bmatrix} r_1^2 & -2r_1r_2 & 0 & r_2^2 & 0 & 0 \\ r_1r_2 & r_1^2 - r_2^2 & 0 & -r_1r_2 & 0 & 0 \\ 0 & 0 & r_1 & 0 & -r_2 & 0 \\ r_2^2 & 2r_1r_2 & 0 & r_1^2 & 0 & 0 \\ 0 & 0 & r_2 & 0 & r_1 & 0 \\ 0 & 0 & 0 & 0 & 0 & 1 \end{bmatrix}.$$

The vector $\mathbf{m}_\theta$ denotes the elements of the seismic moment tensor expressed in the aligned reference system and $\mathbf{R}_{m\theta}$ is a matrix that rotates the seismic moment tensor arranged in column vector form. For the reference system used in this study $r_1 = \cos\theta$ and $r_2 = -\sin\theta$ for a clockwise rotation, and $r_1 = \cos\theta$ and $r_2 = \sin\theta$ for a counterclockwise rotation.

Solving the inversion using equation (6) eliminates the need to rotate the observations each time when a new source with a different hypocenter is introduced (Jechumtalova and Eisner, 2008). The change to the aligned system is accounted for by the matrix $\mathbf{R}_{m\theta}^{-1}$.

Inversion Stability and Acquisition Design

The resolution matrix provides information about the resolvability of the model parameters in terms of the medium property and acquisition geometry. However, it does not explicitly consider the noise content in the observations and uncertainties associated with other inversion-related parameters (e.g., inaccuracies in the medium velocity model). In this section, we evaluate the dependence of the inversion on angular aperture α_1 (Fig. 3) and noise level for single vertical-monitoring well applications.

The parameter of choice for stability evaluation is the condition number (C) of matrix $\mathbf{G}$ (Dufumier and Rivera, 1997). Instead of using the traditional definition, we compute the condition number of $\mathbf{G}$ as

$$C_\epsilon = \lambda_{\max}/\lambda_{\min\neq 0}, \tag{7}$$

where $\lambda_{\max}$ is the largest eigenvalue of $\mathbf{G}$ and $\lambda_{\min\neq 0}$ is the smallest eigenvalue of $\mathbf{G}$ that is different from zero. Under this condition, only eigenvalues related to the five solvable elements of the seismic moment tensor are considered. To compute the condition numbers we formulate the problem using equation (6) and reference the seismic moment tensor in the aligned system. We choose a vertical array of two receivers and vary α_1 from 2° to 60° (see Fig. 3). The azimuth (θ) and the horizontal distance (d) of the line of receivers from the source are randomly selected. Our results show that as α_1 decreases the condition number increases rapidly and thereby lowers the stability of the inversion (see Fig. 3).

To illustrate the process of acquisition design, consider known arbitrary sources with their moment tensors referenced in the aligned system. We perform inversions for five different combinations of random noise level and angle α_1. The problem is solved using the pseudoinverse. For a given combination, the inversion is performed 100 times and a new time series containing Gaussian noise is added to the observations in each iteration. We define the random noise level by normalizing its maximum amplitude to the maximum amplitude of the signal from a single receiver, and then multiply the outcome by the desired percentage. For each combination of α_1 and noise level, we compute a normalized mean squared error (NMSE) via (Fig. 4)

$$\text{NMSE} = \frac{1}{100}\sum_{i=1}^{100}\frac{|\mathbf{m}_i - \mathbf{m}_i'|^2}{|\mathbf{m}_i|^2},$$

where $\mathbf{m}_i'$ is the result of the inversion and $\mathbf{m}_i$ is the true moment tensor in the ith realization of a noise level and α_1; vectors $\mathbf{m}_i'$ and $\mathbf{m}_i$ are moment tensors arranged in vector form. As expected, the NMSE of the inverted solution is zero for noise-free data, but increases with decreasing α_1, when noise is added (see Fig. 4). By setting cutoff values of 100 for C_ϵ and 0.025 for the NMSE, an aperture $\alpha_1 \sim 15°$ is likely too small to lead to stable inversion results when the noise level exceeds 15%. This suggests that, for a line of receivers

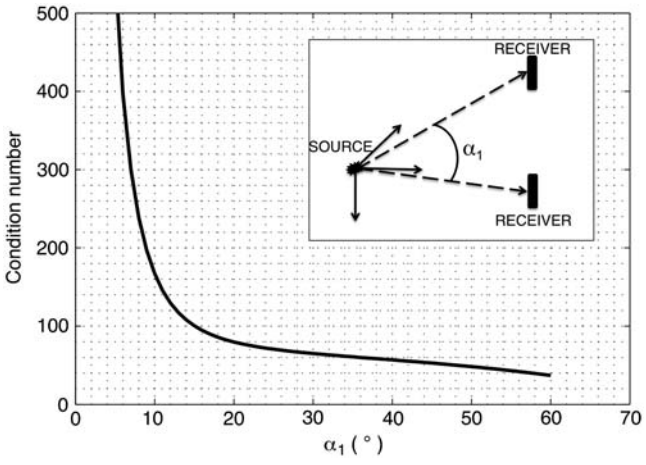

Figure 3. Condition number (C_ϵ) of the matrix $\mathbf{G}$ for different angular apertures between receivers with respect to the source hypocenter (α_1).

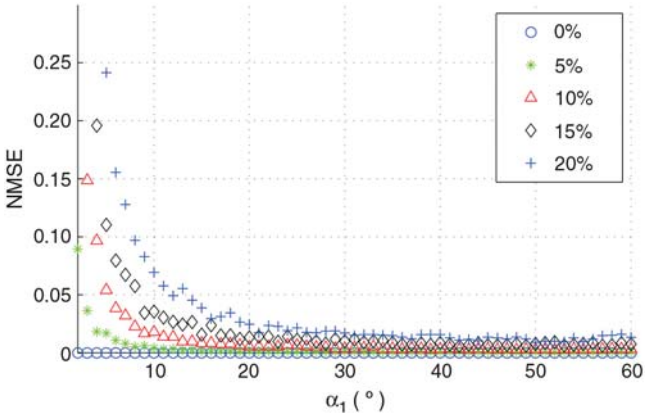

Figure 4. NMSE function of the inversion for different combinations of aperture (α_1) and noise level.

located at 100 m from the source hypocenter, the only receivers contributing to the solution of the inverse problem are those separated by more than ~26 m; the required separation is ~132 m for a line located at 500 m. A 5% perturbation in *P*- and *S*-wave speeds increases the NMSE, then the maximum allowable noise level for a reliable solution decreases to ~10% for α_1 close to 15° (Fig. 5).

It should be noted that this acquisition design requires a case-by-case analysis of the condition number C_ϵ and the NMSE function. The magnitudes of the condition number and the sensitivity to noise depend on the parameterization of the inverse problem. For example, Nolen-Hoeksema and Ruff (2001) adopted the same parameterization used in this study and obtained reliable solutions for condition numbers on the order of 100–500. On the other hand, Dufumier and Rivera (1997) introduced a different parameterization and report a much smaller cutoff value (~5) required for the condition number. The cutoff values for C_ϵ and the NMSE depend on the level of desired accuracy of the solutions.

Minimum Requirements for a Full Moment Tensor Inversion

Stability for Nonvertical Monitoring Geometries

The resolution matrix becomes the identity when a receiver is placed outside a defined observational plane. This full resolvability is only true for noise-free data. For instance, the condition number of the full inversion (6 independent elements of the moment tensor) enables us to determine the minimum relative orientations and distances between receivers. For this part of the analysis, we consider one receiver (R_1) at a fixed distance of 400 m from the source and two receivers (R_2 and R_3) embedded in a plane perpendicular to the straight line between R_1 and the source (Fig. 6). For simplicity, the angle between receivers R_1 and R_2 (similarly for R_1 and R_3) will be referred to as the aperture from the source (α_1), and the angle between receivers R_2 and R_3 with vertex in R_1 will be referred to as the aperture between receivers (α_2). Assuming the same homogeneous medium, it is impractical to explore all possible combinations of receivers outside a single observational plane. However, the magnitude of the distances and orientations required by a full moment tensor solution can be assessed through numerical experiments.

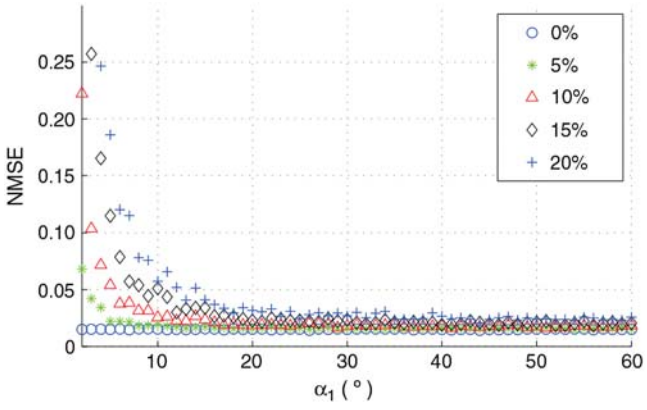

Figure 5. NMSE function of the inversion for different combinations of aperture (α_1) and noise level. The velocity model is biased by an increment of 5% in both *P*- and *S*-wave speeds.

We calculate the condition number of the inversion for multiple combinations of angles α_1 and α_2 for four different acquisition geometries (Figs. 6 and 7). The most stable solution space depends on factors such as the alignment of line R_1-R_2 with the vertical axis of the reference system. A single high resolvability zone is obtained when these two receivers are not aligned (Figs. 7a, 7b, and 7c), and two distinct stability zones are obtained otherwise (Fig. 7d). The azimuth (θ) of the fixed receiver (R_1) also appears to impact the location of maximum resolvability, especially with respect to angle α_2 (Figs. 7a and 7b). In general, angle α_1 attains its optimal value from 40° to 55°. However, while a minimum value for the angle α_1 is required for stability conditions, large angles tend to introduce additional instability after the minimum condition number is reached. Furthermore, the optimal range for α_2 varies significantly for different geometries, despite a consistent increase in condition number near angles 0° and 180° (see the Resolution under Single Vertical-Monitoring Well Geometries section) in all cases.

Sensitivity to Noise and Velocity Perturbation

For the same scenario shown in Figure 7b, we perform inversions under different combinations of random noise level and angles α_1 and α_2. For each combination we obtain solutions for 100 realizations of random noise–moment tensor and compute their NMSE. As expected, higher condition numbers are associated with higher values of NMSE and, for a fixed condition number, the scatter in NMSE increases with the noise level (Fig. 8). These two observations are more evident when condition numbers exceed 100 (not presented here). Furthermore, background velocities have considerable influences on the inversion outcome as, for instance, a 5% perturbation in *P*- and *S*-wave speeds increases the scatter and magnitudes of the NMSE by a factor of 10 (Fig. 9).

Full Moment Tensor Inversion from a Single Deviated Monitoring Well

For microseismic monitoring applications, it is critical to identify the combinations of angles α_1 and α_2 that are (1) practical in borehole experiments, and (2) able to resolve the full moment tensor in an unconstrained inversion. For one of the examples presented in Figure 6, we have shown that various source–receivers geometries can lead to reliable solutions, with condition numbers < 80 for a cutoff NMSE value of 0.025 and a noise level $< 15\%$ (see Figs. 7b and 9). One combination that also meets the two aforementioned objectives is $\alpha_1 = 45°$ and $\alpha_2 = 130°$ (see Fig. 7b). For a fixed receiver located 400 m from the source hypocenter,

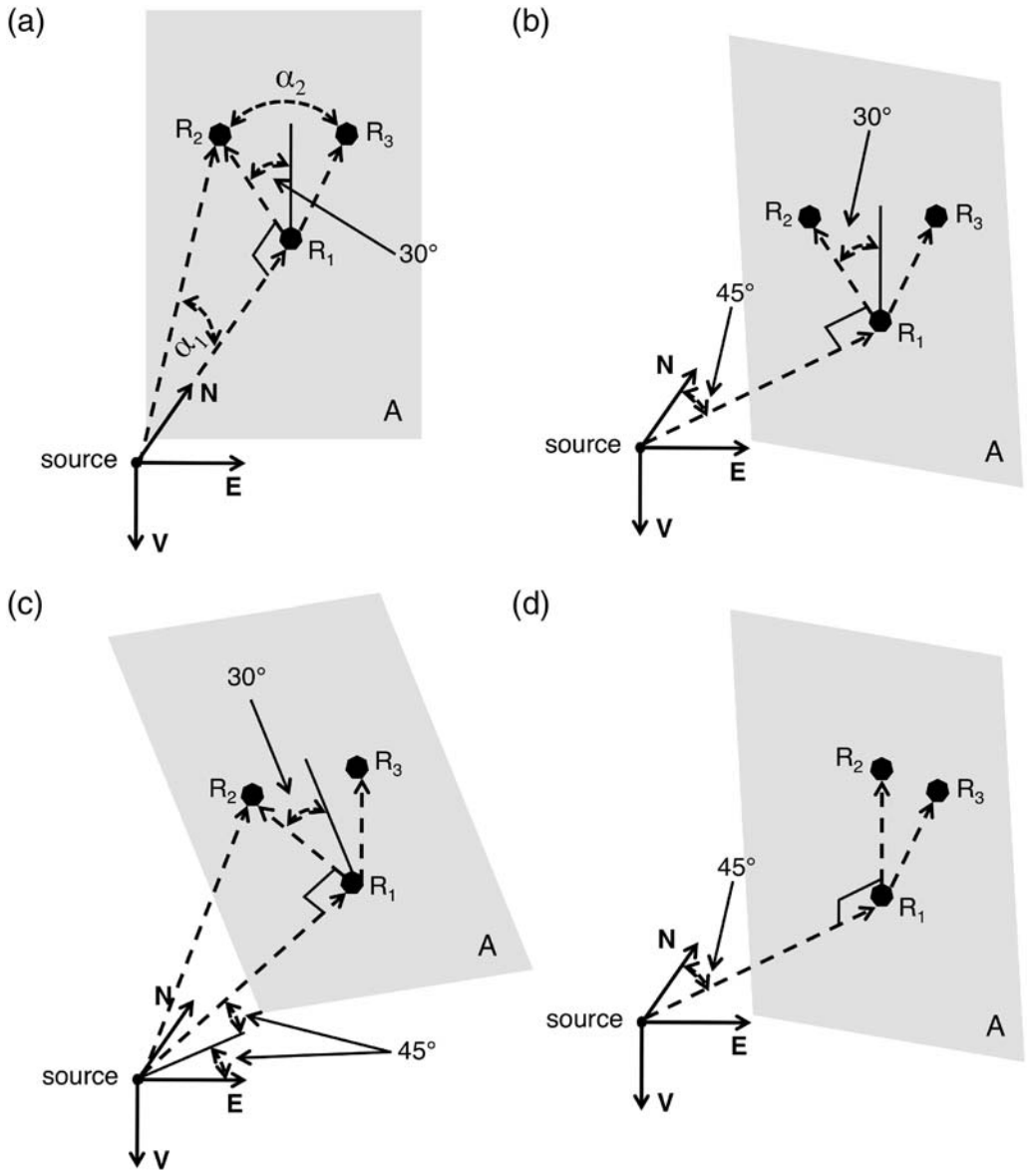

Figure 6. Source–receiver geometry arrangements to compute the condition number for the full source mechanism inversion. Receivers R_1, R_2, and R_3 are contained in the plane A, which lies perpendicular to the line that joins the source hypocenter with R_1. The angle α_1 denotes the aperture between receivers from the source hypocenter and α_2 is the aperture between receivers R_2 and R_3 with respect to R_1. (a) Source hypocenter and receiver R_1 are aligned with an axis of the reference system and the three receivers form a vertical plane. (b) Source hypocenter and receiver R_1 are not aligned with any of the axis of the reference system and the three receivers form a vertical plane. (c) Source hypocenter and receiver R_1 are not aligned with the reference system and the three receivers form a nonvertical plane. (d) Source hypocenter and receiver R_1 are not aligned with the reference system but receivers R_1 and R_2 are aligned in the vertical direction.

the angle α_1 translates to a distance of 400 m between receivers (Fig. 10). Under this configuration, these three receivers form a smooth trajectory that does not exceed a dogleg severity (DLS) of ~6°/30 m (Heisig *et al.*, 2004). Current directional drilling technologies allow the perforation of wells with this degree of curvature (Bryan *et al.*, 2009), and hence the full moment tensor can potentially be extracted from a carefully selected deviated monitoring well.

Monitoring from a deviated well requires information on the volume over which the inversion is stable. Consider the well trajectory from Figure 10 and an acquisition design with nine receivers: the nine receivers are distributed in three groups of three with the central receiver from each group at the locations showed in Figure 10. The remaining two receivers in each group are separated by 5 m from the center. For this monitoring geometry, an isosurface for a condition number of 80 (Fig. 11) exhibits perfect symmetry between the two sides of the well. A relatively complex stability volume is obtained where the approximate spatial limits of x, y, and z are: 100 and 500 m, 200 and −500 m, and 1500 and 1900 m, respectively. Depending on the location of the induced fracture (or fractures), this monitoring geometry

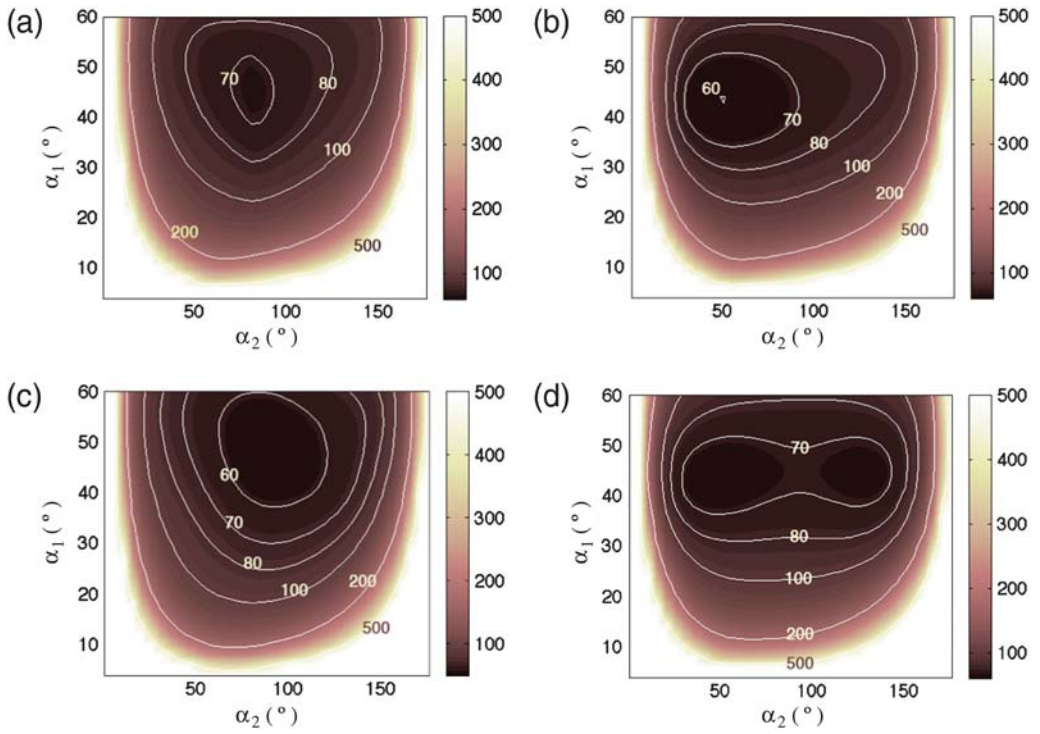

Figure 7. Condition number for different combinations of the angles α_1 and α_2. The four graphs correspond to the source–receiver geometries presented in Figure 6. Condition numbers above 600 are set at 600 for better visualization.

could facilitate moment tensor inversions of at least a significant fraction of induced microseismic events.

Conclusions

We have investigated two important problems associated with microseismic monitoring. We first review the case when the travel-path trajectories are constrained to a plane, where only five of the six elements of the seismic moment tensor are recoverable. The resolution matrix provides a broader overview of the moment tensor resolvability displaying linear correlation between the elements of the moment tensor. According to our simulations, the error due to an incorrect constraint on the dipole perpendicular to the observational plane can only be propagated to two further elements of the moment tensor. On the other hand, all the eigenvalues associated with the sensitivity matrix differ from zero when one or more receivers fall outside the observational plane. This indicates that, in theory, one can resolve all six elements of the seismic moment tensor. However, due to the presence of noise and small eigenvalues, the resulting solutions can be unstable. In this case our analysis based on the condition number of the sensitivity matrix can be highly advantageous. The condition number analysis enables us to access levels of

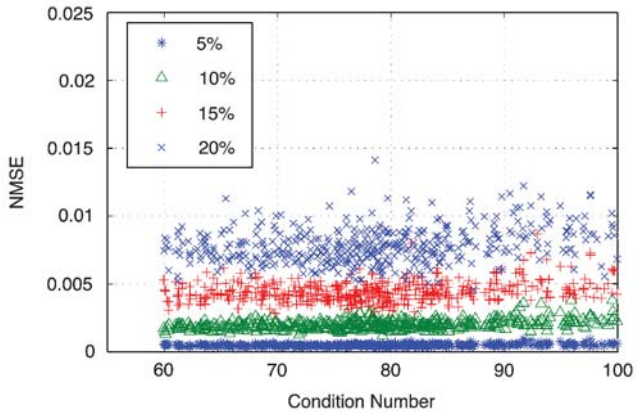

Figure 8. NMSE function for all combinations of α_1 and α_2 with condition number < 100 in Figure 7b. The percent value represents noise level.

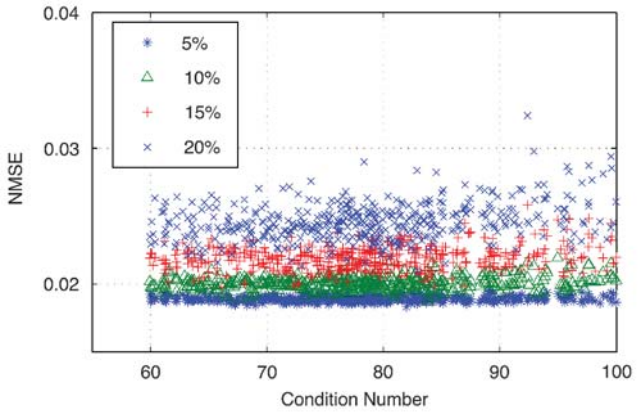

Figure 9. NMSE function for all combinations of α_1 and α_2 with condition number < 100 in Figure 7b. The percent value represents noise level. In this case, the *P*- and *S*-wave speeds are biased by 5%.

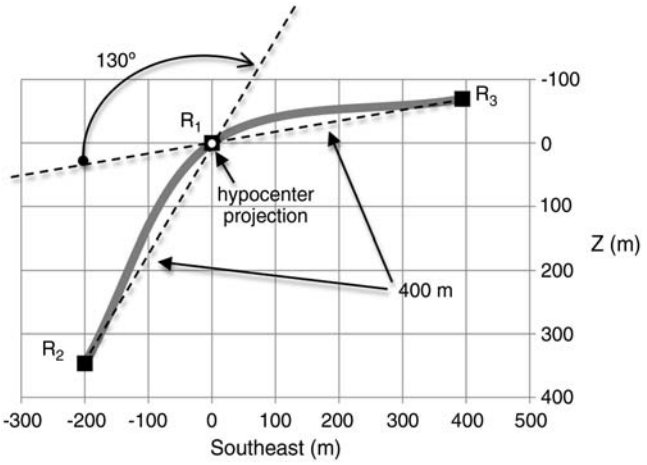

Figure 10. Example of a receivers configuration that can solve the full seismic moment tensor inversion for the given source projection (white dot). Distances are measured over the plain that contains the receivers. The source hypocenter is located at 400 m in the perpendicular direction to this view. The gray line represents a smooth trajectory joining the three receivers.

resolvability for a given acquisition layout. The inversion of the full moment tensor with single borehole data is feasible in situations when the array of receivers is deployed in a deviated well. For instance, our simulations in homogeneous media showed that deviated wells with curvature (DLS) on the order of 6°/30 m can be used to retrieve the full moment tensor. For case studies involving abrupt changes in velocity and/or anisotropy, the condition number analysis can also be an important indicator of the resolvability of the seismic moment tensor prior to monitoring tests.

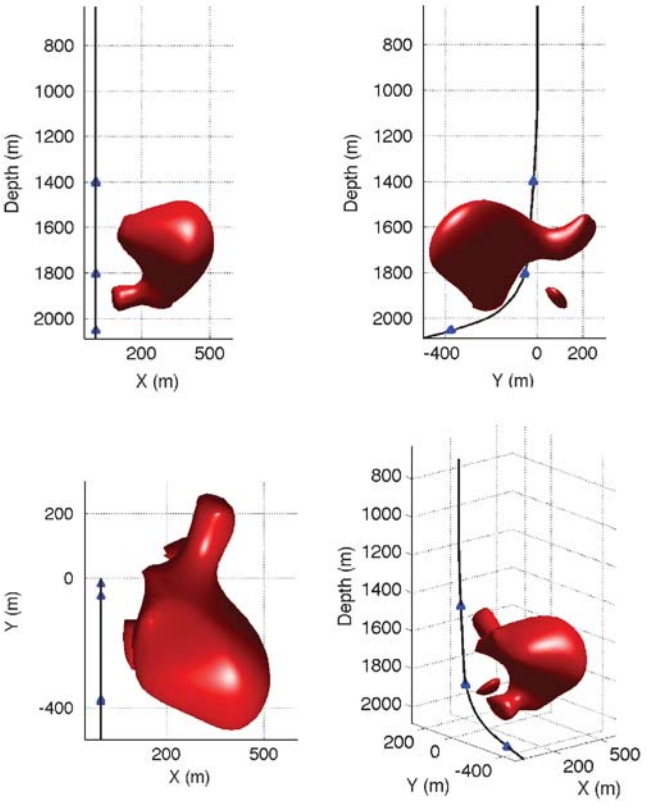

Figure 11. Receiver distribution (blue triangles) along an ideal deviated well (black line) that can solve a full moment tensor inversion. An isosurface value of 80 (condition number) is selected for this plot.

Data and Resources

Synthetic seismograms used in this study were computed with standard ray tracing techniques using formulas from the books of Aki and Richards (2009) and Shearer (1999).

References

Aki, K., and P. Richards (2009). *Quantitative seismology*, University Science Books, Sausalito, California, 700 pp.

Anton, H., and R. Busby (2003). *Contemporary Linear Algebra*, Wiley, New York, 594 pp.

Aster, R., B. Borchers, and C. Thurber (200five). *Parameter estimation and inverse problems*, Elsevier Academic Press, Amsterdam, 301 pp.

Bernardi, F., J. Braunmiller, U. Kradolfer, and D. Giardini (2004). Automatic regional moment tensor inversion in the European-Mediterranean region, *Geophys J Int* **157,** 703–716, doi 10.1111/j.1365-246X.2004.02215.x.

Bleakly, D., J. Wolfe, I. Leslie, M. Prince, V. Shumila, and T. Urbancic (2007). Using multi-well microseismicity to identify fracture types associated with hydraulic fracture stimulations, *CSEG Recorder* **32,** 49–51.

Bryan, S., J. Cox, and D. Blackwell (2009). High-dogleg rotary-steerable systems: A step change in drilling process, Presented at the *SPE Annu. Technical Conf. and Exhibition*, 4–7 October 2009, New Orleans, Louisiana, doi 10.2118/124498-MS.

Dreger, D., and D. Helmberger (1993). Determination of source parameters at regional distances with three-component sparse network data, *J. Geophys. Res.* **98,** no. B5, 8107–8125, doi 10.1029/93JB00023.

Dufumier, H., and L. Rivera (1997). On the resolution of the isotropic component in moment tensor inversion, *Geophys. J. Int.* **131,** no. 3, 595–606, doi 10.1111/j.1365-246X.1997.tb06601.x.

Dziewonski, A., T. Chou, and J. Woodhouse (1981). Determination of earthquake source parameters from waveform data for studies of global and regional seismicity, *J. Geophys. Res.* **86,** no. B4, 2825–2852, doi 10.1029/JB086iB04p02825.

Heisig, G., G. Cavallaro, P. Jogi, J. Hood, and I. Forstner (2004). Continuous borehole curvature estimates while drilling based on downhole bending moment measurements, Presented at the *SPE Annu. Technical Conf. and Exhibition*, 26–29 September 2004, Houston, Texas, doi 10.2118/90794-MS.

Horn, R. A., and C. R. Johnson (1985). *Matrix Analysis*, Cambridge U Press, New York, 561 pp.

Jechumtalova, Z., and L. Eisner (2008). Seismic source mechanism inversion from a linear array of receivers reveals non-double-couple seismic events induced by hydraulic fracturing in sedimentary formation, *Tectonophysics* **460,** 124–133, doi 10.1016/j.tecto.2008.07.011.

Jing, Ch., and T. Rape (2004). Resolvability analysis for rock property inversions of multicomponent seismic data, *SEG Expanded Abstracts* **23,** doi 10.1190/1.1845313.

Kawakatsu, H. (1995). Automated near-realtime CMT inversions, *Geophys. Res. Lett.* **22,** 2569–2572.

Kolinsky, P., L. Eisner, V. Grechka, D. Jurick, and P. Duncan (2009). Observation of shear-wave splitting from microseismicity induced by hydraulic fracturing: A non-VTI story, Presented at the *71st EAGE Conf. and Exhibition*, 8–11 June 2009, Amsterdam, The Netherlands.

Menke, W. (1989). *Geophysical Data Analysis: Discrete Inverse Theory*, Academic Press, San Diego, California, 289 pp.

Nolen-Hoeksema, R., and L. Ruff (2001). Moment tensor inversion of microseisms from the B-sand propped hydrofracture, M-site, Colorado, *Tectonophysics* **336,** 163–181, doi 10.1016/S0040-1951(01)00100-7.

Pasyanos, M. E., D. S. Dreger, and B. Romanowicz (1996). Toward real-time estimation of regional moment tensors, *Bull. Seismol. Soc. Am.* **86,** 1255–1269.

Phillips, W., T. Fairbanks, J. Rutledge, and D. Anderson (1998). Induced microearthquake patterns and oil-producing fracture systems in the Austin chalk, *Tectonophysics* **289,** 153–169.

Rao, Y., Y. Wang, and J. Morgan (2006). Crosshole seismic waveform tomography—II. Resolution analysis, *Geophys. J. Int.* **166,** 1237–1248, doi 10.1111/j.1365-246X.2006.03031.x.

Rutledge, J. T., and W. S. Phillips (2003). Hydraulic stimulation of natural fractures as revealed by induced microearthquakes, Carthage Cotton Valley gas field, east Texas, *Geophysics* **68,** 441–452.

Shearer, P. (1999). *Introduction to Seismology*, Cambridge U Press, New York, 396 pp.

Sileny, J., D. Hill, L. Eisner, and F. Cornet (2009). Non-double-couple mechanisms of microearthquakes induced by hydraulic fracturing, *J. Geophys. Res.* **114,** B08307, 15, doi 10.1029/2008JB005987.

Sipkin, S. (1994). Rapid determination of global moment-tensor solutions, *Geophys. Res. Lett.* **21,** 1667–1670, doi 10.1029/94GL01429.

Trampert, J. (1998). Global seismic tomography: The inverse problem and beyond, *Inverse Prob.* **14,** 371–385, doi 10.1088/0266-5611/14/3/002.

Trifu, C., and V. Shumila (2002). Reliability of seismic moment tensor inversions for induced microseismicity at Kidd Mine, Ontario, *Pure Appl. Geophys.* **159,** 145–164, doi 10.1007/PL00001248.

Tsuruoka, , Hiroshi, Hitoshi Kawakatsu, and Taku Urabe (2009). GRiD MT (grid-based real-time determination of moment tensors) monitoring the long-period seismic wavefield, *Phys. Earth Planet In.* **175,** 8–16, doi 10.1016/j.pepi.2008.02.014.

Van Rijssen, E., and G. Herman (1991). Resolution analysis of band-limited and offset-limited seismic data for plane-layered subsurface models, *Geophys. Prospect.* **39,** 61–76, doi 10.1111/j.1365-2478.1991.tb00301.x.

Vavrycuk, V. (2007). On the retrieval of moment tensors from borehole data, *Geophys. Prospect.* **55,** 381–391, doi 10.1111/j.1365-2478.2007.00624.x.

Vera Rodriguez, I., and M. Sacchi (2009). Resolvability analysis of single azimuth seismic moment tensor inversion, Presented at the *CSPG CSEG CWLS Convention* 476–479.

Wiggins, R. (1972). The general linear inverse problem: Implications of surface waves and free oscillations for Earth structure, *Rev. Geophys. Space Phys.* **10,** 251–285, doi 10.1029/RG010i001p00251.

Xia, J., R. Miller, and Y. Xu (2008). Data-resolution matrix and model-resolution matrix for Raleigh-wave inversion using a damped least-squares method, *Pure Appl Geophys* **165,** 1227–1248, doi 10.1007/s00024-008-0364-2.

Zhao, L., and D. Helmberger (1994). Source estimation from broadband regional seismograms, *Bull. Seismol. Soc. Am.* **84,** 91–104.

Department of Physics and Institute for Geophysical Research
University of Alberta
4-183 CCIS
Edmonton AB, T6G 2E1
Canada
verarodr@ualberta.ca

Manuscript received 12 January 2011